Thermodynamics and Kinetics of Methylglyoxal Dimer Formation: A Computational Study

Hadley E. Krizner, David O. De Haan, and Jeremy Kua*

Department of Chemistry, University of San Diego, 5998 Alcala Park, San Diego, California 92110

Received: April 7, 2009; Revised Manuscript Received: May 5, 2009

Density functional theory (B3LYP//6-311+G*) calculations, including Poisson−Boltzmann implicit solvent and free energy corrections, are applied to study the hydration of methylglyoxal and the subsequent formation of dimeric species in solution. Our calculations show that, unlike glyoxal, fully hydrated species are not thermodynamically favored over their less hydrated counterparts, nor are dioxolane ring species the thermodynamic sink, which is in agreement with experimental data. Instead, we find that aldol condensations are the most favored oligomerization reactions for methylglyoxal. These results differ from those of glyoxal, which, lacking the methyl group, cannot access the enol structure leading to aldol condensation. For methylglyoxal, the product from nucleophilic attack at the aldehyde rather than the ketone was favored. Our results help explain some of the observed differences between methylglyoxal and glyoxal, in particular the different array of oligomers formed.

Introduction

The vast majority of submicrometer aerosol particles in the free troposphere contain organic material, often up to 50% by mass.[1−3] The presence of organic compounds has a strong impact on aerosol particle growth,[4] water uptake, and cloud formation.[5] Because of these effects, organic aerosol material contributes to uncertainty in the prediction of climate change.[6] Most of this organic material is secondary, meaning that it is formed in gas-to-particle transfer processes where the particles may be either cloud droplets or aerosol particles. In urban areas, secondary organic aerosol (SOA) comprises up to 90% of the organic aerosol mass.[7]

Several recent studies have demonstrated that our understanding of SOA formation is far from complete. In both field measurements[8,9] and smog chamber simulations,[10−20] SOA has been shown to contain oligomeric macromolecules that appear to have been formed in particle-phase reactions. In Mexico City, observed SOA formation rates were much higher than model predictions,[21] whereas in the free troposphere, significantly more SOA is present than can be modeled using well-characterized formation pathways.[22] It is clear that important source gases, chemical processes, or both are missing from models and are responsible for significant SOA formation.

In light of this, attention has recently been given to the aerosol-forming potential of the α-dicarbonyl compound methylglyoxal. This compound is commonly found in the troposphere[23] because it is produced by atmospheric oxidation of both anthropogenic and biogenic hydrocarbons.[23−26] With a Henry's law coefficient of 3.71×10^3 $M \cdot atm^{-1}$,[27] it is scavenged by water droplets and is the most common aldehyde after formaldehyde and glyoxal in clouds, dew, and fogwater.[28−33] By assuming that methylglyoxal uptake into clouds and aerosol is irreversible and governed by an uptake coefficient measured for glyoxal ($\alpha = 0.0029$[34]), Fu et al.[23] estimated that methylglyoxal could form as much as 8 $Tg \cdot C \cdot yr^{-1}$ SOA, mostly via cloud uptake. This was more than a quarter of the total global SOA formed and three times more SOA than was formed by glyoxal in their model. Interestingly, methylglyoxal uptake coefficients have been measured ($\alpha = 0.0076$[35] and 0.023[36]) and are larger than that assumed by Fu et al.,[23] so their estimate of SOA formation from methylglyoxal is not a strict upper limit. Despite this potential importance, the atmospheric chemistry of methylglyoxal has received comparatively little study, and its SOA formation mechanisms are not fully characterized.

One known pathway to SOA formation by methylglyoxal is oxidation in clouds. The aqueous-phase rate constant for reaction with OH radical is 1.1×10^9 $M^{-1} \cdot s^{-1}$,[37] and low-volatility reaction products such as pyruvic acid and oligomers formed in aldol condensation reactions have been identified.[20] However, because only a fraction of methylglyoxal would be oxidized in a single cloud event,[38] other chemical processes may be of equal or greater importance if they also form low-volatility products that remain behind as cloud-processed aerosol when a cloud droplet evaporates.

Oligomer formation is one such competing chemical process. Methylglyoxal is known to form oligomers in drying aqueous solutions. Paulsen et al.[16] measured methylglyoxal oligomer formation rates in nebulizer-generated aerosol with a volatility tandem differential mobility analyzer. They observed oligomer formation without oxidant or irradiation and noted that the oligomer formation rate was similar to that observed in photooxidation experiments on α-pinene in the presence of NO_x and water vapor. Oligomer formation has also been detected by laser desorption mass spectrometry in bulk solutions of methylglyoxal and methylglyoxal/aldehyde mixtures that were dried as a part of the sample preparation process.[39] Although no structural data was obtained, acetal oligomer structures built on dioxolane rings were proposed to explain the collected mass spectra. Loeffler et al.[40] detected oligomer formation in evaporating methylglyoxal solutions by attenuated total reflectance Fourier transform infrared spectroscopy. Because C−O stretching peaks assigned to dioxolane rings were not observed, open oligomer acetal structures were instead proposed. Nemet et al.[41] detected many oligomer peaks in DMSO solutions of freeze-dried methylglyoxal but not in aqueous solutions. A few of these peaks were tentatively assigned to a cyclic trioxane acetal trimer and to an acetal dimer with a dioxane ring structure (structure **9** in Figure 3).

* Corresponding author. E-mail: jkua@sandiego.edu.

10.1021/jp903213k CCC: $40.75
Published on Web 05/29/2009

Other studies have probed the direct uptake of methylglyoxal by aerosol. In flow tube experiments with bulk, concentrated sulfuric acid/water mixtures, Zhao et al.[35] observed that methylglyoxal uptake decreased with increasing acidity. They interpreted this as evidence that methylglyoxal uptake depended on water content and that hydration and acetal oligomerization were more important processes than (acid-catalyzed) aldol condensation under these conditions. However, in chamber experiments with aqueous ammonium sulfate and ammonium sulfate/sulfuric acid aerosol, Kroll et al.[42] did not observe any methylglyoxal uptake by AMS and only very minimal uptake by SMPS. The seeming discrepancy between the two studies has not been resolved, and it is not clear whether methylglyoxal can be taken up directly by atmospheric aerosol.

To summarize, the existing experimental studies provide strong evidence that methylglyoxal can form SOA during cloud processing both by aqueous-phase oxidation and by reacting with itself in drying solutions, forming various oligomers. Because structural experimental evidence is indirect and very limited, the formation of acetal oligomers has been proposed on the basis of an analogy to glyoxal.

There have been several computational studies that probe the mechanism and products formed by glyoxal and methylglyoxal oligomerization. Tong et al.[43] used quantum mechanical methods to suggest that glyoxal forms acetal oligomers linked by dioxolane rings, which is in agreement with experimental data. Our quantum mechanical study of glyoxal[44] complemented this study by providing kinetic data (reaction barriers) and the structures of transition states and relevant intermediates, showing that the hydrated dioxolane ring dimer is the thermodynamic sink for dimerization and thus the crucial intermediate prior to forming the dioxolane ring trimer. Barsanti and Pankow[45] used empirical and Benson thermochemical data and applied thermodynamic principles to conclude that under atmospheric conditions, glyoxal could form acetal oligomers, whereas methylglyoxal could form oligomers by aldol condensation reactions, suggesting that the reactions of methylglyoxal may differ from those expected from studies of glyoxal chemistry.

The goal of our current study is to determine by quantum mechanics the most thermodynamically favorable reaction pathways, intermediates, and products in the oligomerization of methylglyoxal. As discussed in the Computational Methods section, our methods result in a close match with experimental data for hydration of methylglyoxal in solution, that is, formation of monohydrate and dihydrate in a 60 to 40% distribution.[41] In contrast, glyoxal is fully hydrated in solution.[44] In the Results and Discussion section, we show that the most prominent difference between glyoxal and methylglyoxal is that the favored products for glyoxal are dioxolane ring acetal dimers, whereas for methylglyoxal, the aldol condensation products from enol attack on the aldehyde are favored overall. Whereas glyoxal oligomerization favors the formation of five-membered acetal ring structures relative to the monomer, the corresponding acetal oligomer structures for methylglyoxal have higher free energies relative to the monomer. In contrast, the aldol condensation reaction of methylglyoxal is thermodynamically favored and results in oligomers that can easily undergo continued polymerization to form a complicated mixture of organic species. Glyoxal cannot access these reactions because they require a proton shift from the methyl group to form the enol structure. Our calculations support the suggestion of Barsanti and Pankow[45] that the aldol condensations are the most thermodynamically favored reactions for methylglyoxal.

Computational Methods

All calculations were carried out using Jaguar 6.0[46] at the B3LYP[47−50] flavor of density functional theory (DFT) with a 6-311G** basis set. To maximize the probability of finding the global minimum, we performed calculations on various conformers of each structure with different internal hydrogen bond networks. Higher energy conformers are included only where relevant in the discussion. Raw data for the electronic energy of the optimized gas phase structures, Poisson−Boltzmann (PB) solvation energy, zero-point energy (ZPE), and thermodynamic corrections to 298 K are available in Table S1 in the Supporting Information.

The PB continuum approximation[51,52] was used to describe the effect of solvent. In this approximation, a smooth solvent-accessible surface of the solute is calculated by rolling a sphere of radius R_{solv} (1.40 Å for water) over the van der Waals surface. The solvent is represented as a polarizable continuum surrounding the molecule with dielectric constant, ε (80.4 for water). Charges are allowed to develop on the surface according to the electrostatic potential of the solute and ε; then, the polarized reaction field of the solvent acts back on the quantum mechanical description of the solute. The wave function of the complex is relaxed self-consistently with the reaction field to solve the PB equations. Whereas the forces on the quantum mechanical solute atoms due to the solvent can be calculated in the presence of the solvent, in this work, the solvation energy was calculated at the optimized gas-phase geometry for all structures at minima. This is because there is practically no change between the gas phase and the implicit solvent-optimized geometries. It is important to note that even though the solvation energy contribution is to some extent a free-energy correction, it certainly does not account for all of the free energy. Comparisons with different electronic structure methods and implicit solvents are provided in the Supporting Information.

The analytical Hessian was calculated for each optimized geometry in the gas phase. The DFT gas-phase energy was then corrected for zero-point vibrations. Negative eigenvalues in transition-state calculations were not included in the ZPE. A scaling factor of ~0.97 typically used at the B3LYP level for the vibrational energies was not included. This could potentially result in an energy difference of up to 0.7 kcal·mol^{-1} in the system studied, although the difference will be much smaller after the addition of the entropic correction. The temperature-dependent enthalpy correction term is straightforward to calculate from statistical mechanics. Assuming that the translational and rotational corrections are a constant times kT, that low frequency vibrational modes will generally cancel out when calculating enthalpy differences, and that the vibrational frequencies do not change appreciably in solution, we can calculate H_{298K}. (See Table S1 in Supporting Information.)

The corresponding free-energy corrections in solution are much less reliable.[53−55] Changes in free-energy terms for translation and rotation are poorly defined in solution, particularly as the size of the molecule increases. Additional corrections to the free energy for concentration differentials among species (to obtain the chemical potential) can be significant, especially if the solubility varies among the different species in solution. Furthermore, because the reactions being studied are in solution, the free energy being accounted for comes from two different sources: thermal corrections and implicit solvent. Neither of these parameters is easily separable, nor do they constitute all of the required parts of the free energy under our approximations of the system.

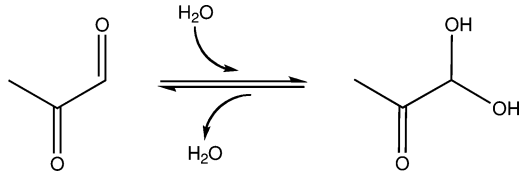

Figure 1. First hydration of methylglyoxal.

To estimate the free energy, we followed the method of Lau and Deubel,[56] who included the solvation entropy of each species as half of its gas-phase entropy. Wertz[57] and Abraham[58] had previously suggested that upon dissolving in water, molecules lose a constant fraction (~0.5) of their entropy. In this study, we found that using this 0.5 fraction entropy correction for ΔG values provides results that are comparable to experimental data for glyoxal oligomerization. A discussion of this can be found in our previous study of glyoxal.[44] Because relevant reactions of methylglyoxal take place in solution, we include this solvation entropy correction in our ΔG values throughout the remainder of the article. Therefore, the ΔG values given in this study include the ZPE, temperature correction to 298 K, and the solvation energy and entropy corrections for all reactions in solution.

Our calculations of ΔG are stoichiometric, where water is often one of the reactants. In the first hydration of methylglyoxal to form the monohydrate shown in Figure 1, equally dilute concentrations (because of the implicit solvent approximation) of both reactants are assumed in the calculations. To compare directly with experimental data, we need to account for the different concentrations of each reactant. This concentration correction was determined from the following equation

$$\Delta G = \Delta G^{\circ} + RT \ln([\text{products}]/[\text{reactants}])$$

For the first hydration of methylglyoxal in ~1 M solution at 298 K, the equation is

$$\Delta G_{\text{concn}} = \Delta G + RT \ln([\text{monohydrate}]/[\text{methylglyoxal}][\text{water}])$$

where ΔG is the change in free energy for the stoichiometric reaction. Because the concentration of water in a 1 M solution of methylglyoxal is ~55 M

$$\Delta G_{\text{concn}} = \Delta G + RT \ln[(1)/(1)(55)]$$

which gives

$$\Delta G_{\text{concn}} = \Delta G - 2.37 \text{ kcal/mol}$$

For the second hydration of methylglyoxal, the reactants are water and the monohydrate. Because there are two water molecules when this reaction is referenced back to methylglyoxal, the equations are now

$$\Delta G_{\text{concn}} = \Delta G + RT \ln([\text{dihydrate}]/[\text{methylglyoxal}][\text{water}]^2)$$

$$\Delta G_{\text{concn}} = \Delta G + RT \ln[(1)/(1)(55)^2]$$

$$\Delta G_{\text{concn}} = \Delta G - 4.74 \text{ kcal/mol}$$

To our knowledge, there is very little experimental thermodynamic data for the hydration of methylglyoxal. When methylglyoxal is dissolved in water to make a 0.598 M solution (at 298 K), the monohydrate and dihydrate are present in a 60:40 ratio, respectively.[31] We see that our ΔG_{concn} values for the hydration of methylglyoxal correspond to this experimental ratio, as shown in Figure 2. The ΔG values for the stoichiometric (equal concentration) reactions are included for comparison.

For both the stoichiometric and concentration-corrected ΔG values, the monohydrate has the lowest free energy and is therefore the thermodynamic sink. For the first hydration, ΔG_{concn} is significantly negative, showing again that the monohydrate is favored overall and that very little of the dehydrated species remains in solution. For the dihydrate, ΔG_{concn} is marginally positive, showing that the second hydration requires only a slight increase in free energy. We can infer that the mono- and dihydrate species are present in nearly equal amounts in solution. The 60:40 ratio determined experimentally gives $K_{\text{eq}} = 3/2 = 1.5$, which corresponds to $\Delta G_{\text{exptl}} = +0.24$ kcal/mol, which is very close to our calculated value of +0.3 kcal/mol.

However, concentrations of intermediates in complex oligomerization reactions will change continuously as these reactions proceed. In addition, one of the aims of our study of methylglyoxal was to make direct comparisons with glyoxal, for which ΔG_{concn} values were not included.[44] Therefore, in the present study, all data and discussions will be in terms of ΔG, the value corresponding to stoichiometric reactions. From our previous work using the same computational methodology and entropy approximation, we found that for the hydration of aldehydes, our calculated ΔG values are within 1 kcal/mol of experimental values, and our calculated $\Delta G^{\ddagger}$ values overestimate the experimental value by approximately 3 kcal/mol.[44] Corresponding data in terms of ΔG_{concn} and ΔH for all reactions can be found in the Supporting Information.

Results and Discussion

We have divided our analysis into the four different types of reactions: hydration, acetal dimerization, ring closure, and aldol condensation. The first three reactions are summarized in Figure 3, and the aldol condensation is summarized in Figure 4. Note that the free energies in Figures 3 and 4 are relative to methylglyoxal and water as the reference state, whereas those in Tables 1−3 are for the reactions listed in the left column of each table. Therefore, the reader interested in the global energetics should use Figures 3 and 4. The entries in Tables 1−3 conveniently calculate the differences for the reader interested in a particular chemical reaction. Geometries of the reactants, products, intermediates, and transition states in Cartesian coordinates are provided in the Supporting Information.

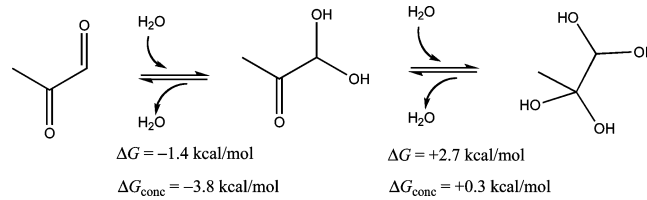

Figure 2. Overall free energies for methylglyoxal hydration.

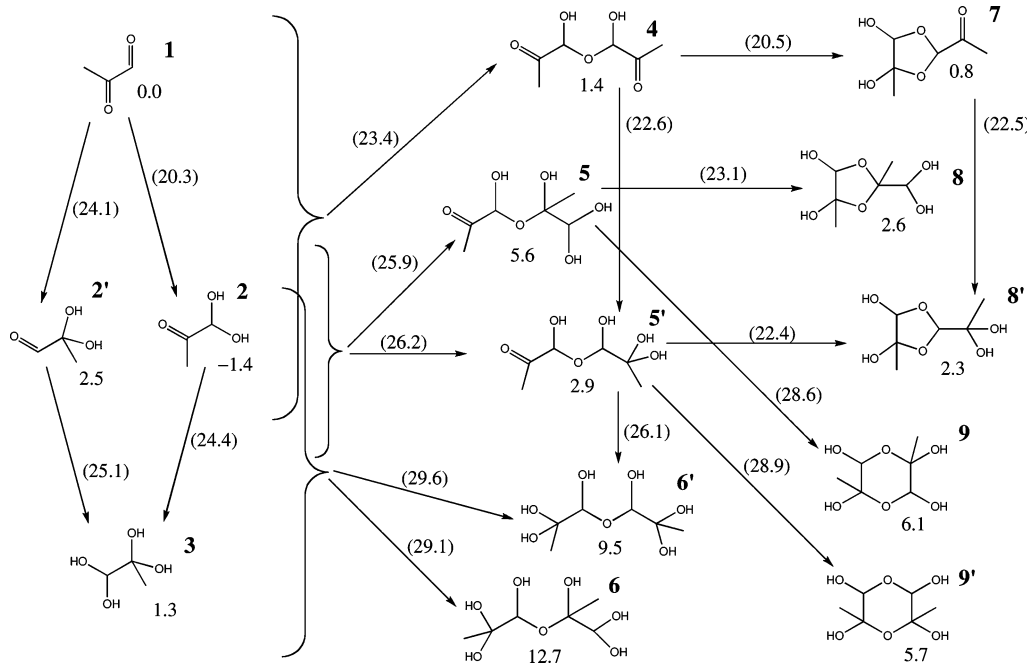

Figure 3. Overall free energy landscape of hydration, dimerization, and ring closure pathways (ΔG in kcal/mol).

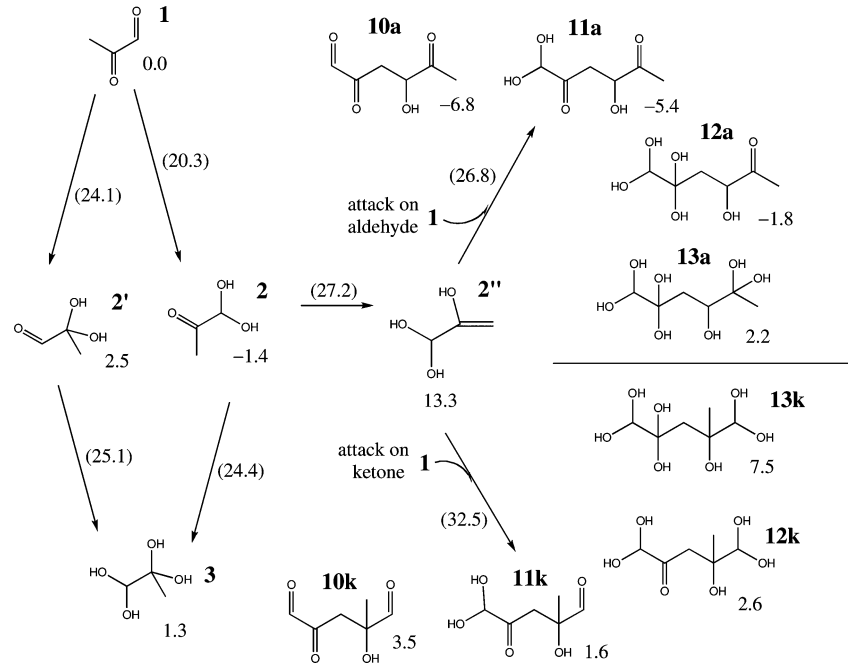

Figure 4. Overall free energy landscape of aldol condensation reactions (ΔG in kcal/mol).

TABLE 1: ΔG and $\Delta G^{\ddagger}$ (in kilocalories per mol) for Hydration Reactions

reaction	ΔG (kcal/mol)	$\Delta G^{\ddagger}$ (kcal/mol)	transition state
1 + H_2O → **2**	−1.4	20.3	**H1**
1 + H_2O → **2′**	2.5	24.1	**H1′**
2 + H_2O → **3**	2.7	25.9	**H2**
2′ + H_2O → **3**	−1.2	22.7	**H2′**

TABLE 2: ΔG and $\Delta G^{\ddagger}$ (in kilocalories per mol) for Dimerization Reactions

reaction	ΔG (kcal/mol)	$\Delta G^{\ddagger}$ (kcal/mol)	transition state
1 + **2** → **4**	2.9	24.8	**D12**
2 + **2** → **5**	8.4	28.8	**D22**
2′ + **2** → **5′**	1.9	25.2	**D2′2**
2 + **3** → **6**	12.9	29.3	**D23**
2′ + **3** → **6′**	5.8	25.9	**D2′3**

Hydration. Hydration reactions are represented by the vertical down arrows in Figure 3. On the basis of the raw energies in Table S1 (Supporting Information), we can calculate ΔG and $\Delta G^{\ddagger}$ for each hydration reaction. Values for each individual reaction are given in Table 1. The addition of one water molecule converts **1** to its monohydrates **2** and **2′**, depending on whether the aldehyde or ketone is hydrated. For the aldehyde hydration, $\Delta G = -1.4$ kcal/mol, and for the ketone hydration, $\Delta G = +2.5$ kcal/mol. Therefore, hydration of the aldehyde leads to the favorable monohydrate, as expected. Subsequent hydration of either **2** or **2′** leads to the dihydrate, **3**.

The monohydrate **2** is the dominant monomeric species in solution because the formation of **2′** and the dihydrate **3** require

TABLE 3: ΔG and $\Delta G^{\ddagger}$ (in kilocalories per mol) for Ring Closure Reactions

reaction	ΔG (kcal/mol)	$\Delta G^{\ddagger}$ (kcal/mol)	transition state
4 → **7**	−0.6	19.1	**R7**
5 → **8**	−3.0	17.8	**R8**
5 → **9**	0.6	23.0	**R9**
5′ → **8′**	−0.6	19.5	**R8′**
5′ → **9′**	2.8	26.0	**R9′**

hydration of a ketone group, which is unfavorable in comparison with the aldehyde hydration. This is in agreement with experimental data; when DMSO was added to freeze-dried, solid methylglyoxal, the monohydrate **2** was the dominant species in solution. For stoichiometric ratios, our calculated free energy of **2** is 1.4 and 2.7 kcal/mol more stable than that of **1** and **3**, respectively. However, when a ∼0.6 M solution of methylglyoxal was made by dissolving in water, there was a ∼60:40 ratio of the monohydrate **2** to the dihydrate **3**.[41] In this case, our calculated free energy of **2** is 0.3 kcal/mol more stable than that of **3**. These latter results correspond to our data with the inclusion of the concentration correction, ΔG_{concn}, as described in the Computational Methods section.

The hydration reactions resulted in six-centered transition states with two additional water molecules, similar to those in our previous study of glyoxal.[44] The transition-state structures for **H1** and **H2** are shown in Figure 5. The barriers for the hydration reactions range from 20−26 kcal/mol. The barrier for the first aldehyde hydration is the lowest of these at $\Delta G^{\ddagger} = +20.3$ kcal/mol. In summary, only the first hydration of the aldehyde is thermodynamically favorable, which again points to **2** as the dominant monomer species in solution and a key starting point for dimerization reactions.

Acetal Dimerization. Individual acetal dimerization reaction energies are summarized in Table 2, and their pathways are shown as the first set of horizontal arrows connecting the left and middle panels in Figure 3. Dimerization of **1** to form **4** with the addition of one water molecule to the transition state was not calculated explicitly because such a reaction would have a high barrier, as was determined from our study of glyoxal.[44]

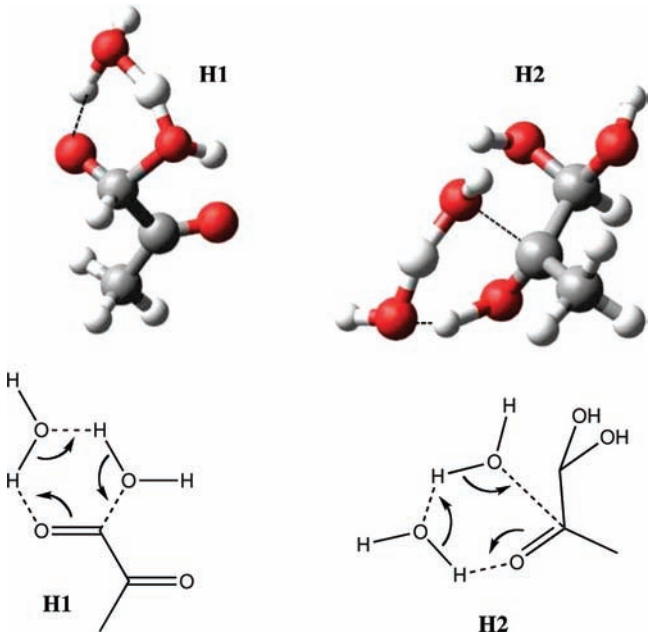

Figure 5. Monomer hydration transition-state structures **H1** and **H2**.

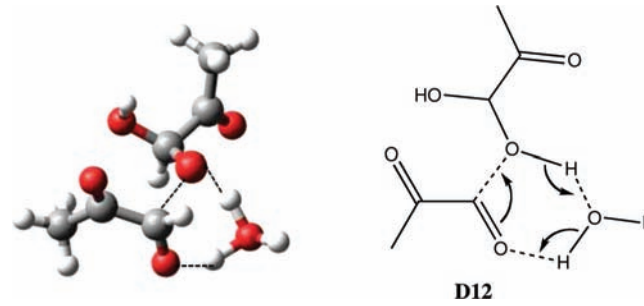

Figure 6. Dimerization transition-state structure **D12**.

Dimerization of **1** and **2**, with the sp^3 hydroxyl oxygen on **2** acting as the nucleophile, has a barrier of 24.8 kcal/mol. This reaction results in a six-center transition state with one additional water molecule. The structure is shown for **D12** in Figure 6.

Because there are two possible monohydrates, **2** and **2′**, the dimerization reactions for methylglyoxal are more complex than those of glyoxal and can follow two separate pathways. The pathway involving the monohydrate **2** is expected to be favored because of the higher concentration of **2** in solution. The structures designated with a prime follow the less favorable pathway involving the hydrated ketone **2′**, which is in lower concentration in solution.

Dimerization of **2** yields **5**, with $\Delta G = +8.4$ kcal/mol, whereas dimerization of **2′** and **2** yields **5′**, with $\Delta G = +1.9$ kcal/mol. Reactions of the mono- and dihydrate follow a similar pattern. Dimerization of **2** and **3** yields **6**, with $\Delta G = +12.9$ kcal/mol, whereas dimerization of **2′** and **3** yields **6′**, with $\Delta G = +5.8$ kcal/mol. These dimerization six-center transition states (**D22**, **D2′2**, **D23**, and **D2′3**) are similar to **D12**. Dimerization of **3** is not likely to occur and was not calculated explicitly because of the high barrier determined in the corresponding dihydrate dimerization of glyoxal[44] because the sp^2 carbon presents a better electrophile than the sp^3 carbon; this would apply to both glyoxal and methylglyoxal dimerization reactions. (For glyoxal, it was found that the most favorable pathway for this reaction involved prior dehydration of one of the hydrated carbons to form the monohydrate).

Table 2 summarizes the dimerization reactions. All dimerization reactions are uphill, and the fully dehydrated species **4** is the most thermodynamically favored open dimer under stoichiometric conditions, as shown in Figure 3 where all free energies are referenced to methylglyoxal and water as the reactants. A higher concentration of water would favor the hydrated species (as shown in the Supporting Information). Subsequent hydrations of **4** are unfavorable because they require the hydration of a ketone, which is consistent with the data from the hydration of the monohydrate **2**. This differs from our previous result with glyoxal, in which subsequent hydration of dimers is favorable because an aldehyde is being hydrated in all cases. The range of barriers is 25−29 kcal/mol for dimerization (Table 2) when referenced to the different reactants. When the common reference of methylglyoxal and water is chosen, the free energies of these transition states ranges from 23 to 29 kcal/mol. (See Figure 3).

Ring Closure. Ring closure reaction energies are summarized in Table 3, and their pathways are shown connecting the middle and right panels in Figure 3. Two favorable ring structures can be formed via intramolecular nucleophilic attack on the sp^2 carbon: the five-membered dioxolane ring dimer and the six-membered dioxane ring dimer. The formation of both rings is thermodynamically favorable with **4** forming **7**, **5** forming **8** and **9**, and **5′** forming **8′** and **9′**. Because ring closure involves

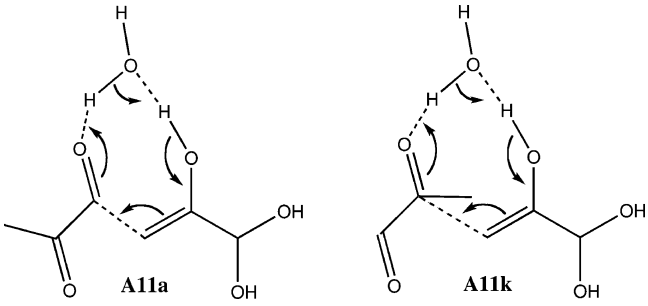

Figure 7. Aldol condensation transition states **A11a** and **A11k**.

nucleophilic attack on a carbonyl similar to dimerization, temporary dehydration of **6** and **6′** to **5** and **5′** is expected prior to ring formation when a high concentration of water is present.

The most favorable ring structure for methylglyoxal is **7**, which was expected on the basis of our previous results from glyoxal, in which the dioxolane ring dimer was the thermodynamic sink. The dehydrated structure **7** is favorable because, as shown with the hydration reactions, it is unfavorable to hydrate the ketone under stoichiometric conditions. We observe that **8′** is marginally more stable (within the computational error) than **8**.

Ring closures resulted in six-center transition states. Ring closures forming **7**, **8**, and **8′** ($\Delta G^{\ddagger}$ values for **R7**, **R8**, and **R8′** are +19.1, +17.8, and +19.5 kcal/mol, respectively) have significantly lower barriers than those forming **9** and **9′** ($\Delta G^{\ddagger}$ is +23.0 kcal/mol for **R9** and +26.0 kcal/mol for **R9′**). Table 3 summarizes the ring closure reaction energies. In agreement with the hydration and dimerization reactions, subsequent hydration of the ketone group of **7** (to form **8**) is uphill, making **7** the most favored ring structure. The free energies of these transition-state structures with reference to methylglyoxal and water (Figure 3) are 21−23 kcal/mol for forming dioxolane rings and ∼29 kcal/mol for forming dioxane rings. From the free-energy landscape in Figure 3, we see that acetal dimerization and ring closure reactions remain uphill overall compared with the methylglyoxal monomer (and the monohydrate **2**), which is in contrast with glyoxal, where oligomeric ring structures were thermodynamically favored over the monomer.[44]

Aldol Condensation. Methylglyoxal can form oligomers through aldol condensation reactions via proton shift from the methyl group of the monohydrate (**2**) forming the enol structure **2″**, as shown in Figure 4. Because the enol is +14.7 kcal/mol higher in free energy, it is not easily accessed, however several of the aldol condensation products are found to be thermodynamically favorable overall. Aldol condensation products result from nucleophilic attack of the terminal sp^2 carbon in the enol on the carbonyl carbon of either an aldehyde or a ketone. As shown in Figure 4, attack of the enol **2″** on the aldehyde of **1** leads to the product **11a**, whereas attack on the ketone of **1** leads to the product **11k**. The lowest-energy transition states for these two reactions were eight-center transition states, as shown in Figure 7. From Figure 4, we see that attacking the aldehyde results in a transition state that is significantly lower in energy (+26.8 kcal/mol) compared with attacking a ketone (+32.5 kcal/mol).

In a solution of monomeric methylgloxal, **1** is the lowest-energy structure with an aldehyde group, so if the enol was to attack an aldehyde containing species, **1** would be more likely than **2′**. However, **2** is the lowest-energy structure containing a ketone group. The enol attack on the ketone of **2** to form **12k** has a transition-state energy (not shown in Figure 4) of +32.1 kcal/mol, which is practically similar to the attack on **1** to form

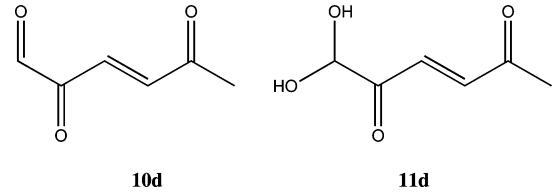

Figure 8. Dehydrated aldol structures **10d** and **11d** with central C═C.

11k. Therefore, we chose just to represent the transition states **A11a** and **A11k** in Figure 7 (with relative energies shown in Figure 4) because this gives a direct comparison of the enol attacking different carbonyls of the same molecule.

The structures **10a**, **12a**, and **13a**, can be accessed by dehydration or hydration of **11a**. Similarly, the structures **10k**, **12k**, and **13k** can be accessed by dehydration or hydration of **11k** (where **a** and **k** designate products obtained by attack on the aldehyde and ketone, respectively). Each set of four structures is related by successive hydrations. (**10** is the fully dehydrated structure, whereas **13** is the fully hydrated structure.) The hydration and dehydration barriers are ∼21 kcal/mol for hydrating an aldehyde and ∼24 kcal/mol for hydrating a ketone, as discussed in the previous section on hydration reactions.

The products formed from nucleophilic attack on the aldehyde are favored over those formed by attack on the ketone. The favored aldol condensation product is **10a**. The aldol condensation products **10a**−**12a** are also the thermodynamic sink for all monomers and dimers of methylglyoxal from a comparison of the global ΔG values in Figures 3 and 4. Structures **10a** and **11k** are the most stable products for the aldehyde and ketone, respectively. In the aldol condensation, carbon−carbon bond formation results in products retaining longer hydrocarbon chains and no formation of acetals and hemiacetals. This contributes to their stability over the hemiacetal dimerization products **4**−**6**. The more thermodynamically favored structures **10a**−**13a** also have an unbranched hydrocarbon chain, whereas **10k**−**13k** have one methyl branch. Interestingly, under stoichiometric conditions, the dehydrated species **10a** is the most favorable, with its single aldehyde remaining unhydrated. For attack at the ketone, the most favorable structure **11k** keeps one of the two aldehydes unhydrated.

The two lowest energy structures **10a** and **11a** could potentially lose a water molecule across one of the central carbon−carbon bonds to form a delocalized π system. These structures, designated **10d** and **11d**, are shown in Figure 8. The dehydration process is marginally uphill. With reference to methylglyoxal and water, the free energies of **10d** and **11d** are −3.0 and −4.9 kcal/mol, respectively, slightly higher than those of **10a** and **11a** (−6.8 and −5.4 kcal/mol, respectively; Figure 4).

Overall Reaction Pathways. For the two types of methylglyoxal oligomerization reactions (acetal dimerization and aldol condensation), those that do not access the enol structure are marginally unfavorable, whereas those going through the enol structure to form aldol condensation products are thermodynamically favorable. Furthermore, aldol condensation products can lead to subsequent oligomerization when enol structures continue to attack the aldehyde or ketone of oligomers already formed. Alternatively, thermodynamically favorable products such as **10a**, **11a**, and **12a** could "enolize" and add more methylglyoxal units. This corresponds to experimental and kinetic modeling data for methylglyoxal in which a large range of oligomers is formed.[45] These results differ from our study of glyoxal,[44] which lacks the methyl group that would allow it

to access the enol structure. Therefore glyoxal cannot participate in aldol condensation reactions, and its oligomerization typically stops at its thermodynamic sink, the dioxolane ring trimer.

The landscape is complicated by several facts: (1) the equilibrium concentration of the enol structure is small, (2) the free energy of the keto−enol tautomerization transition state and the aldol condensation transition state (**A11a**) are higher than the lowest dimerization transition state (**D12**) and comparable to two other dimerizations (**D22**, **D2′2**), and (3) any terminal acetyl group can "enolize"; that is, besides **2**, a number of low-energy structures with acetyl groups (**10a**−**12a**, **4**, **5**, **5′**, **7**) can further oligomerize via aldol condensation. The result is that a large variety of structures can potentially be formed, and this will depend heavily on the reaction conditions. Predicting product distributions under different conditions would require a detailed kinetic analysis in a reaction network model beyond the scope of this article. A crude and simple estimation of rate constants can be found in the Supporting Information.

The route to the dioxolane rings has lower barriers overall compared with the aldol condensation products, but the latter are thermodynamically more stable. A mixture of both types of reactions is possible because both routes can be accessed at each point in the oligomerization; aldol condensate dimers that are not fully hydrated (**10**−**12**) could undergo intramolecular nucleophilic attack to form ring structures, whereas nonaldol dimers (**4**, **5**, **5′**) and ring structures (**7**) that contain an acetyl group can tautomerize and undergo aldol condensation. Hydration and dehydration reactions also have barriers that are comparable to oligomerization; the majority of these barriers are in the 20−27 kcal/mol range. In contrast, for glyoxal,[44] the hydration and dehydration barriers were lower (in the 15−19 kcal/mol range), and fully hydrated structures were thermodynamically favored and therefore the only ones observed. Our calculated free-energy landscapes (Figures 3 and 4) for methylglyoxal, however, suggest that in methylglyoxal, the product distribution (aldol condensates, dioxolane rings, or even just the monomeric species of methylglyoxal) is highly sensitive to the reaction conditions.

The flow tube uptake experiments of Zhao et al.[35] were conducted with residence times of less than 0.1 s and total surface exposure times of 1 to 2 min. Their observation that methylglyoxal uptake increased with the water content of the condensed H_2O/H_2SO_4 bulk phase, which they attributed to acetal polymer formation, is consistent with our results for a system under kinetic control because the kinetic barriers to acetal formation are lower than those for aldol condensation. The chamber uptake experiment of Kroll et al.[42] was more likely to access thermodynamically favored products because it was conducted over many hours and at higher temperature than almost all of the experiments of Zhao et al. Using their gas-phase methylglyoxal concentration of ∼1 ppm and the effective Henry's law coefficient $H^* = 3710\ \mathrm{M \cdot atm^{-1}}$, the concentration of methylglyoxal in the aerosol is predicted to reach only 3.7 mM, which is too low to increase particle volumes detectably and too low for methylglyoxal to participate effectively in aldol condensation self-reactions. In addition, the low, steady-state uptake rates observed by Zhao et al.[35] at reaction times in excess of 1 min would cause only marginal increases in aerosol particle volumes that would be difficult to detect in a chamber study like that of Kroll et al.[42]

Conclusions

Our study has applied DFT methods to determine energies of reactions for hydration, dimerization, ring closure, and aldol condensation of methylglyoxal. By calculating energies of reactions and barriers, we were able to trace the reaction pathways and predict the most viable mechanisms. We found that for methylglyoxal, hydrations of the aldehyde are favored over hydrations of the ketone. Therefore, the monohydrate **2** is the dominant species in solution. Acetal dimerization reactions of methylglyoxal are uphill, in contrast with the downhill dimerization of glyoxal. For methylglyoxal oligomerizations that do not proceed through the enol structure, we found that the dioxolane ring **7** is most favorable. However, in contrast with glyoxal, methylglyoxal can access the enol structure and aldol condensation reactions. We found that the aldol condensation products are the thermodynamic sink for methylglyoxal oligomerization. In stoichiometric calculations, aldol condensation product **10a** is the most favorable oligomer. However, the energy landscape is complicated because the kinetically favorable reactions are not those that lead to the thermodynamic sink. Therefore, depending on the reaction conditions, different products could be favored. These include the monomeric species, dehydrated open dimers or dioxolane rings, and aldol condensates; this may explain why different experimental probes have led to a wide variety of observed product distributions. Our calculated free energies of the thermodynamics and barriers can be used as a starting point for a detailed kinetic analysis in a reaction network model to predict product distributions under different conditions.

Acknowledgment. This research was supported by an American Chemical Society Petroleum Research Fund grant (PRF no. 46700-GB10), a Camille and Henry Dreyfus Foundation Start-up Award, and NSF grant ATM-0749145.

Supporting Information Available: Raw energies, Cartesian coordinates for all optimized structures, a comparison of our computational method with other methods, and a crude estimation of rate constants for key reactions. This material is available free of charge via the Internet at http://pubs.acs.org.

References and Notes

(1) Zhang, Q.; Stanier, C. O.; Canagaratna, M. R.; Jayne, J. T.; Worsnop, D. R.; Pandis, S. N.; Jimenez, J. L. *Environ. Sci. Technol.* **2004**, *38*, 4797–4809.

(2) Murphy, D. M.; Cziczo, D. J.; Froyd, K. D.; Hudson, P. K.; Matthew, B. M.; Middlebrook, A. M.; Peltier, R. E.; Sullivan, A.; Thomson, D. S.; Weber, R. J. *J. Geophys. Res.* **2006**, 111.

(3) Zhang, Q.; Canagaratna, M. R.; Jayne, J. T.; Worsnop, D. R.; Jimenez, J. L. *J. Geophys. Res.* **2005**, 110.

(4) Wehner, B.; Petäjä, T.; Boy, M.; Engler, C.; Birmili, W.; Tuch, T.; Wiedensohler, A.; Kulmala, M. *Geophys. Res. Lett.* **2005**, *32*, L171810.

(5) Charlson, R. J.; Seinfeld, J. H.; Nenes, A.; Kulmala, M.; Laaksonen, A.; Facchini, M. C. *Science* **2001**, *292*, 2025–2026.

(6) IPCC 2007 Summary for Policymakers. In *Climate Change 2007: The Physical Science Basis. Contribution of Working Group I to the Fourth Assessment Report of the Intergovernmental Panel on Climate Change*; Solomon, S., Qin, D., Manning, M., Chen, Z., Marquis, M., Averyt, K. B., Tignor, M., Miller, H. L., Eds.; Cambridge University Press: New York, 2007.

(7) Lim, H.-J.; Turpin, B. J. *Environ. Sci. Technol.* **2002**, *36*, 4489–4496.

(8) Denkenberger, K. A.; Moffett, R. C.; Holocek, J. C.; Rebotier, T. P.; Prather, K. A. *Environ. Sci. Technol.* **2007**, *41*, 5439–5446.

(9) Kalberer, M.; Sax, M.; Samburova, V. *Environ. Sci. Technol.* **2006**, *40*, 5917–5922.

(10) Gao, S.; Ng, N. L.; Keywood, M.; Varutbangkul, V.; Bahreini, R.; Nenes, A.; He, J.; Yoo, K. Y.; Beauchamp, J. L.; Hodyss, R. P.; Flagan, R. C.; Seinfeld, J. H. *Environ. Sci. Technol.* **2004**, *38*, 6582–6589.

(11) Iinuma, Y.; Boege, O.; Gnauk, T.; Herrmann, H. *Atmos. Environ.* **2004**, *38*, 761–773.

(12) Baltensperger, U.; Kalberer, M.; Dommen, J.; Paulsen, D.; Alfarra, M. R.; Coe, H.; Fisseha, R.; Gascho, A.; Gysel, M.; Nyeki, S.; Sax, M.; Steinbacher, M.; Prevot, A. S. H.; Sjoegren, S.; Weingartner, E.; Zenobi, R. *Faraday Discuss.* **2005**, *130*, 265–278.

(13) Paulsen, D.; Dommen, J.; Kalberer, M.; Prévôt, A. S. H.; Richter, R.; Sax, M.; Steinbacher, M.; Weingartner, E.; Baltensperger, U. *Environ. Sci. Technol.* **2005**, *39*, 2668–2678.
(14) Angove, D. E.; Fookes, C. J. R.; Hynes, R. G.; Walters, C. K.; Azzi, M. *Atmos. Environ.* **2006**, *40*, 4597–4607.
(15) Dommen, J.; Metzger, A.; Duplissy, J.; Kalberer, M.; Alfarra, M. R.; Gascho, A.; Weingartner, E.; Prévôt, A. S. H.; Verheggen, B.; Baltensperger, U. *Geophys. Res. Lett.* **2006**, *33*, L13805.
(16) Paulsen, D.; Weingartner, E.; Alfarra, M. R.; Baltensperger, U. *J. Aerosol Sci.* **2006**, *37*, 1025–1051.
(17) Hearn, J. D.; Smith, G. D. *Int. J. Mass Spectrom.* **2006**, *258*, 95–103.
(18) Tolocka, M. P.; Jang, M.; Ginter, J. M.; Cox, F. J.; Kamens, R. M.; Johnston, M. V. *Environ. Sci. Technol.* **2004**, *38*, 1428–1434.
(19) Gao, S.; Keywood, M.; Ng, N. L.; Surratt, J.; Varutbangkul, V.; Bahreini, R.; Flagan, R. C.; Seinfeld, J. H. *J. Phys. Chem. A* **2004**, *108*, 10147–10164.
(20) Altieri, K. E.; Seitzinger, S. P.; Carlton, A. G.; Turpin, B. J.; Klein, G. C.; Marshall, A. G. *Atmos. Environ.* **2008**, *42*, 1476–1490.
(21) Volkamer, R.; Jimenez, J. L. *Geophys. Res. Lett.* **2006**, *33*, L17811.
(22) Heald, C. L.; Jacob, D. J.; Park, R. J.; Russell, L. M.; Huebert, B. J.; Seinfeld, J. H.; Liao, H.; Weber, R. J. *Geophys. Res. Lett.* **2005**, *32*, L18809.
(23) Fu, T.-M.; Jacob, D. J.; Wittrock, F.; Burrows, J. P.; Vrekoussis, M.; Henze, D. K. *J. Geophys. Res.* **2008**, *113*, D15303.
(24) Jang, M.; Kamens, R. M. *Environ. Sci. Technol.* **2001**, *35*, 3626–3639.
(25) Spaulding, R. S.; Schade, G. W.; Goldstein, A. H.; Charles, M. J. *J. Geophys. Res.* **2003**, *108*, 4247.
(26) Tuazon, E. C.; MacLeod, H.; Atkinson, R.; Carter, W. P. L. *Environ. Sci. Technol.* **1986**, *20*, 383–387.
(27) Betterton, E. A.; Hoffman, M. R. *Environ. Sci. Technol.* **1988**, *22*, 1415–1418.
(28) Matsumoto, K.; Kawai, S.; Igawa, M. *Atmos. Environ.* **2005**, *39*, 7321–7329.
(29) Igawa, M.; Munger, J. W.; Hoffmann, M. R. *Environ. Sci. Technol.* **1989**, *23*, 556–561.
(30) Munger, J. W.; Jacob, D. J.; Daube, B. C.; Horowitz, L. W.; Keene, W. C.; Heikes, B. G. *J. Geophys. Res.* **1995**, *100*, 9325–9333.
(31) Collett, J. L., Jr.; Daube, B. C.; Gunz, D.; Hoffmann, M. R. *Atmos. Environ.* **1990**, *24*, 1741–1757.
(32) van Pinxteren, D.; Plewka, A.; Hofmann, D.; Muller, K.; Kramberger, H.; Svrcina, B.; Bachmann, K.; Jaeschke, W.; Meters, S.; Collett, J. L., Jr. *Atmos. Environ.* **2005**, *39*, 4305–4320.
(33) Steinberg, S.; Kaplan, I. R. *Int. J. Environ. Anal. Chem* **1984**, *18*, 253–266.
(34) Liggio, J.; Li, S.-M.; McLaren, R. *J. Geophys. Res.* **2005**, *110*, D10304.
(35) Zhao, J.; Levitt, N. P.; Zhang, R.; Chen, J. *Environ. Sci. Technol.* **2006**, *40*, 7682–7687.
(36) Saxena, P.; Hildemann, L. M. *J. Atmos. Chem.* **1996**, *24*, 57–109.
(37) Ervens, B.; Gligorovski, S.; Hermann, H. *Phys. Chem. Chem. Phys.* **2003**, *5*, 1811–1824.
(38) Ervens, B.; Feingold, G.; Frost, G. J.; Kreidenweis, S. M. *J. Geophys. Res.* **2004**, *109*, D15205.
(39) Kalberer, M.; Paulsen, D.; Sax, M.; Steinbacher, M.; Dommen, J.; Prevot, A. S. H.; Fisseha, R.; Weingartner, E.; Frankevich, V.; Zenobi, R.; Baltensperger, U. *Science* **2004**, *303*, 1659–1662.
(40) Loeffler, K. W.; Koehler, C. A.; Paul, N. M.; De Haan, D. O. *Environ. Sci. Technol.* **2006**, *40*, 6318–6323.
(41) Nemet, I.; Vikiæc-Topiæc, D.; Varga-Defterdaroviæc, L. *Bioorg. Chem.* **2004**, *32*, 560–570.
(42) Kroll, J. H.; Ng, N. L.; Murphy, S. M.; Varutbangkul, V.; Flagan, R. C.; Seinfeld, J. H. *J. Geophys. Res.* **2005**, *110*, D23207.
(43) Tong, C.; Blanco, M.; Goddard, W. A. I.; Seinfeld, J. H. *Environ. Sci. Technol.* **2006**, *40*, 2333–2338.
(44) Kua, J.; Hanley, S. W.; De Haan, D. O. *J. Phys. Chem. A* **2008**, *112*, 66–72.
(45) Barsanti, K. C.; Pankow, J. F. *Atmos. Environ.* **2005**, *39*, 6597–6607.
(46) *Jaguar*, version 6.0; Schrodinger, LLC: Portland, OR, 2005.
(47) Becke, A. D. *J. Chem. Phys.* **1993**, *98*, 5648–5652.
(48) Becke, A. D. *Phys. Rev. A* **1988**, *38*, 3098–3100.
(49) Vosko, S. H.; Wilk, L.; Nusair, M. *Can. J. Phys* **1980**, *58*, 1200–1211.
(50) Lee, C.; Yang, W.; Parr, R. G. *Phys. Rev. B* **1988**, *37*, 785–789.
(51) Tannor, D. J.; Marten, B.; Murphy, R.; Friesner, R. A.; Sitkoff, D.; Nicholls, A.; Ringnalda, M.; Goddard, W. A., III; Honig, B. *J. Am. Chem. Soc.* **1994**, *116*, 11875–11882.
(52) Marten, B.; Kim, K.; Cortis, C.; Friesner, R. A.; Murphy, R. B.; Ringnalda, M. N.; Sitkoff, D.; Honig, B. *J. Phys. Chem.* **1996**, *100*, 11775–11788.
(53) Wiberg, K. B.; Bailey, W. F. *J. Am. Chem. Soc.* **2001**, *123*, 8231–8238.
(54) Nielsen, R. J.; Keith, J. M.; Stoltz, B. M.; Goddard, W. A., III *J. Am. Chem. Soc.* **2004**, *126*, 7967–7974.
(55) Florian, J.; Warshel, A. *J. Phys. Chem. B* **1998**, *102*, 719–734.
(56) Lau, J. K.-C.; Deubel, D. V. *J. Chem. Theory Comput.* **2006**, *2*, 103–106.
(57) Wertz, D. H. *J. Am. Chem. Soc.* **1980**, *102*, 5316–5322.
(58) Abraham, M. H. *J. Am. Chem. Soc.* **1981**, *103*, 6742–6744.

JP903213K